

# Molecular-dynamics Study on Crack Growth Behavior Relevant to Crystal Nucleation in Amorphous Metal

R. Matsumoto<sup>1</sup>, M. Nakagaki<sup>1</sup>, A. Nakatani<sup>2</sup> and H. Kitagawa<sup>3</sup>

**Abstract:** In this paper, the internal structure-changes around the crack-tip and the pertinent crack growth behavior in an amorphous metal were studied by a molecular dynamics (MD) simulation. In order to perform a large scale calculation, the domain decomposition method was used for parallel calculation. The Finnis-Sinclair potential for  $\alpha$ -iron was used to describe the interatomic potential. Computed results show that nano-scaled crystalline phase grows around the crack-tip. The distribution of deformation zones and deformation mechanism are significantly altered. While grains are relatively small, they are not deformed, and the most amorphous-crystal interfaces have a large strain for phase transition. The emission of dislocations from the near crack-tip is observed after the crystal phase covered the crack-tip surfaces. Although CTOD obtained from MD analysis agrees to Dugdale's model very well during the amorphous state, the crack opening behavior changes remarkably after the crystallization.

**keyword:** Molecular dynamics, amorphous, crystallization, nano-metal, fracture mechanics, deformation mechanism, nano-crystal

## 1 Introduction

Amorphous metal has been spotlighted as an innovative material in the engineering field because of its inherent high strength and a lot of unique properties. As to its production, only the form of a thin film was possible, however the recent developments of the innovative production technology has made it possible to produce metallic

glass of 1~100mm thickness [Inoue (2000)]. And amorphous structured metals are thought to be increasingly employed in industrial products

In recent studies in the literature, it has been reported that nano-sized particles are precipitated due to plastic deformations in amorphous metal or metallic glass [Nieh, Wadsworth, Liu, Ohkubo, and Hirotsu (2001); Ogura, Sato, Tarumi, Shimojo, Takashima, and Higo (2001); Gao, Hackenberg, and Shiflet (2001); Lee, Lee, and Lee (2003); Lee, Kim, Ahn, Kim, Lee, and Lee (2004)]. Their results suggest that the strength of the amorphous metal is much related to evolving crystalline phase during fracture process. It is becoming more important to estimate the mechanical properties of materials with higher accuracy by accounting for such a microscopic internal structure change for predicting stability of structural materials and the micro-mechanical integrity of miniaturized electric parts. Nevertheless, the phenomenon of the deformation induced nano-crystallization and its effect on fracture are not fully understood yet, which is mainly due to the extreme difficulty of experimental observation of the atomic structure changes in the amorphous, since the deformation induced crystallization arising inside the material is in a thermodynamically inequilibrium condition.

In practice, various kinds of nano-metals, which are compound of nano-scaled structures consisting of amorphous and crystal phases, have been developed in recent efforts [Inoue, Nakazato, Kawamura, and Masumoto (1994); Conner, Dandliker, and Johnson (1998); Yoshizawa, Oguma, and Yamauchi (1988)]. As nano-metals are mainly produced by means of a thermal treatment, it might become possible to control the internal structure of nano-metals by the use of deformation-induced crystallization. In order to estimate the mechanical property of nano-metals, it is also necessary to clarify the behavior of crystalline particles in the amorphous phase.

We have hitherto been conducting on the deformation

<sup>1</sup> Department of Mechanical Information Engineering, Faculty of Computer Science and Systems Engineering, Kyushu Institute of Technology 680-4 Kawazu, Iizuka-City, Fukuoka 820-8502, Japan

<sup>2</sup> Department of Adaptive Machine Systems, Graduate School of Engineering, Osaka University 2-1 Yamada-Oka, Suita-City, Osaka 565-0871, Japan

<sup>3</sup> Department of Energy and Mechanical Engineering, Faculty of Engineering, Doshisha University, 1-3 Tatara Tsudani, Kyotanabe-City, Kyoto 610-0394, Japan

mechanism and fracture in the amorphous metal by molecular dynamics (MD) simulations. Those include the analysis on the initial crack opening behavior [Matsumoto, Kitagawa, Nakatani, and Nakatani (2001); Matsumoto, Nakatani, and Kitagawa (2003)]. The work is extended to show that the crystallization is caused by a large deformation, and discussed the transition of the deformation mechanism and the relationship between the deformation condition and the grain shape and size [Matsumoto, Kitagawa, and Nakatani (2003a, 2002)]. Also observed was the Ostwald's crystal growth after precipitation. The MD study on the deformation-induced crystallization has also been performed by use of the "second-nearest neighbor modified embedded atom method"(2NN-MEAM) for Ni [Lee, Baskes, Kim, and Cho (2001); Lee, Kim, Ahn, Kim, Lee, and Lee (2004)]. They showed that the crystallization is much prompted by deformation. In relation to the work, we also found the fact that the tensile hydrostatic stress encourages the crystal nucleation, while the compressive hydrostatic stress accelerates the crystal growth [Matsumoto, Kitagawa, and Nakatani (2003b)]

In case of cracked medium, it is expected that the characteristic crystallization might occur during crack growth for the singular stress distribution and deformation state near the crack tip, and the fracture behavior is changed notably because of the interaction between amorphous and crystal phases. In this paper, a large scale MD simulation of crack growth is performed in order to collect information on the atomic rearrangements. The internal structural phenomena in severely deformed zones are investigated and the consequent changes of fracture behavior caused by deformation-induced nano-crystallization in an amorphous metal are studied.

## 2 MD simulation and analysis model

MD is a simulation method which can estimate various properties of materials by tracing trajectories of all particles in a system by numerically solving Newton's equations. The recent rapid progress of computer performance and the development of the interatomic potential theory have enabled us to treat various kinds of problems by employing a large scale MD. Moreover, various evaluation techniques of mechanical parameters and local structures also have been developed [Shen and Atluri (2004a,b); Nakatani, Nakatani, Sugiyama, and Kitagawa (2000); Honeycutt and Andersen (1988)]. The cou-

pling techniques between the atomistic and continuum models are also expanding the scope [Shen and Atluri (2004c); Abraham (2000)]. The literatures shown in the following are a part of works that provide significant results regarding deformation mechanism and fracture of materials [Buehler, Abraham, and Gao (2003); Kalia, Nakano, Vashishta, Rountree, Van Brutzel, and Ogata (2003); Shastry and Farkas (1996); Nakatani, Shimokawa, Matsumoto, and Kitagawa (2004); Li and Yip (2002); Nishimura and Miyazaki (2001); Schiøtz and Jacobsen (2003); Schiøtz, Tolla, and Jacobsen (1998)].

In order to perform a large scale simulation, we use the domain decomposition method in the parallel calculation. The velocity Verlet's method [Verlet (1967)] and the velocity scaling scheme are respectively used to govern the time evolution and to control temperature.

In the present crack growth simulation, the amorphous metal model for Fe is assumed, in which the interatomic force is derived from the Finnis-Sinclair (FS) potential [Finnis and Sinclair (1984, 1986)]. In FS potential, the total potential energy  $E_P$  is written as following.

$$E_P = E_{N\text{-body}} + E_{\text{pair}} \quad (1)$$

Here,  $E_{N\text{-body}}$  is the  $N$ -body term and  $E_{\text{pair}}$  is the pair-potential part.

$$E_{N\text{-body}} = \sum_i f(\rho_i) \quad (2)$$

$$E_{\text{pair}} = \frac{1}{2} \sum_{i,j} V(R_{ij}) \quad (3)$$

$\rho_i$  is the local electronic charge density at site  $i$ , and  $R_{ij}$  is the distance between atom  $i$  and  $j$ .

The sequence of the process in the analysis modeling undertaken in this study is shown in the following.

### 1. Formation of amorphous plate

A plate of an amorphous metal was numerically produced by a melting-rapid quenching simulation which was used in Ref. Nakatani, Nakatani, Sugiyama, and Kitagawa (2000). During the process, the periodic three-dimensional boundary condition was adopted and Parrinello-Rahman's algorithm was used [Parrinello and Rahman (1981)]. MD simulations usually require large calculation resources. However MD analysis sometimes requires higher calculation costs for the data analysis than

MD simulation itself. In this research, we deal with a quasi three-dimensional model by taking the small thickness in order to reduce the calculation and to avoid the difficulty of data analysis. The size of the amorphous plate is  $104.6 \text{ nm} \times 104.6 \text{ nm} \times 1.74 \text{ nm}$ , containing 1,555,200 atoms. It was confirmed that the amorphous plate does not contain clusters of bcc, fcc and hcp-crystal structures by common neighbor analysis (CNA) [Honeycutt and Andersen (1988)].

## 2. Fabrication of disk model

A disk whose radius is  $R = 50 \text{ nm}$  was cut out from the amorphous plate. The boundary region fixed during the simulation was defined, as shown in Figure 1 by the shaded area within  $R_b = 0.7 \text{ nm}$  distance from the outer edge. The atoms in the constrained region are called as “boundary atom”. The total number of atoms is in the domain  $N = 1,117,086$ , while that in the boundary is  $N_b = 31,117$ .

## 3. Setting of initial crack

In order to analyze the crack growth characteristics in an infinite domain, the crack-tip was initially assumed to be located at the center of the disk. And then a crack was introduced into the disk by giving each atom a set of displacements  $\vec{u} = (u_1, u_2)$  that correspond to the linear elastic solution with mode I stress intensity factor  $K_0^I = 0.4 \text{ MPa}\sqrt{\text{m}}$  under plane strain condition. In the process, the elastic properties (Young’s modulus  $E = 146.4 \text{ GPa}$  and Poisson’s ratio  $\nu=0.26$ ) obtained from the simulation of uniaxial tensile deformation are used [Nakatani, Kitagawa, and Nakatani (1997)].

## 4. Coordinates and periodic boundary condition

The origin is set at the crack-tip, *i.e.* at the center of the disk, whereas the x-axis is directed ahead of the tip in the crack plane, and the z-axis in the thickness direction. The periodic boundary condition (P.B.C.) was enforced on the faces normal to the z-direction, so that it is deformed under semi-plane-strain condition where averaged longitudinal strain component is zero ( $\overline{\epsilon_z}=0$ ).

## 5. Initial temperature

The initial velocities were given to all atoms according to the Maxwell’s distribution at  $T_0 = 600 \text{ K}$ . The melting point of the material is  $T_m = 2,565 \text{ K}$ . Therefore the relative temperature is  $T_r \equiv T_0/T_m = 0.234$ . We found that the deformation-induced nano-crystallization is possible also in the case the initial temperature is low, however it needs a large deformation [Matsumoto, Kitagawa, and Nakatani (2003a, 2002)]. The purpose of this paper is to show the influence of the crystallization on the crack growth behavior, thus the initial temperature was set relatively high.

## 6. Relaxation

A calculation for relaxation was performed during 100 ps under 600 K. The boundary atoms were fixed during the calculation. The crack closure over the surface from the crack-tip  $\Delta a_r = 6.2 \text{ nm}$  was recognized during the relaxation. The entire structure of the domain after the relaxation is shown in Figure 2.

## 7. Crack growth simulation

The boundary atoms were moved with the equivalent velocity in accordance with the increasing rate of stress intensity factor  $\dot{K}^I = 2 \times 10^9 \text{ MPa}\sqrt{\text{m}}/\text{s}$ . The average velocity of the boundary atoms is  $v_{\text{ave}} \simeq 2.998 \text{ m/s}$  (The maximum and minimum velocity are  $v_{\text{max}} \simeq 4.545 \text{ m/s}$  and  $v_{\text{min}} \simeq 1.464 \text{ m/s}$ , respectively). During the crack growth simulation, the thickness of the model was fixed. For the subsequent detailed data analysis, stress components, coordinates and potential energy of each atom averaged over 1 ps were output every 10 ps. The present MD simulation was performed up to  $t = 1,200 \text{ ps}$  ( $K^I = 2.8 \text{ MPa}\sqrt{\text{m}}$ ).

## 3 Result and discussions

### 3.1 Energy profile of the system

Figure 3 shows the changes of the potential energy, the kinetic energy and the total energy of the system since the initial state. Time evolution of the total energy is equivalent to the external work. The figure also shows the measure of temperature change of the system converted from the kinetic energy. The potential energy gradually increases and starts to decrease rapidly at around  $t = 700 \text{ ps}$ . The sudden increase of the temperature corresponds to the reduction of the potential energy, and it

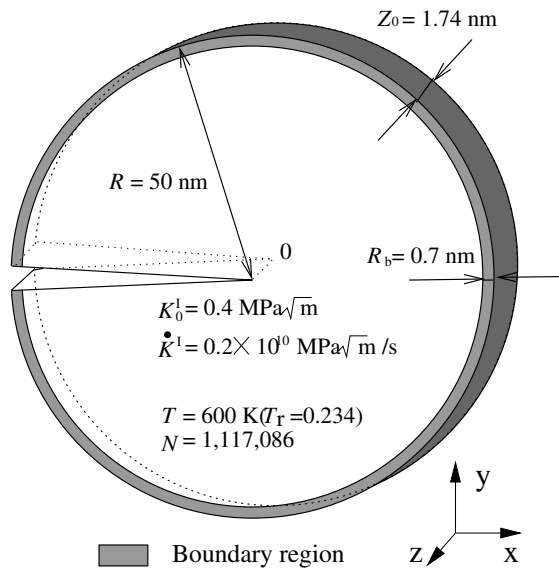


Figure 1 : Simulation model

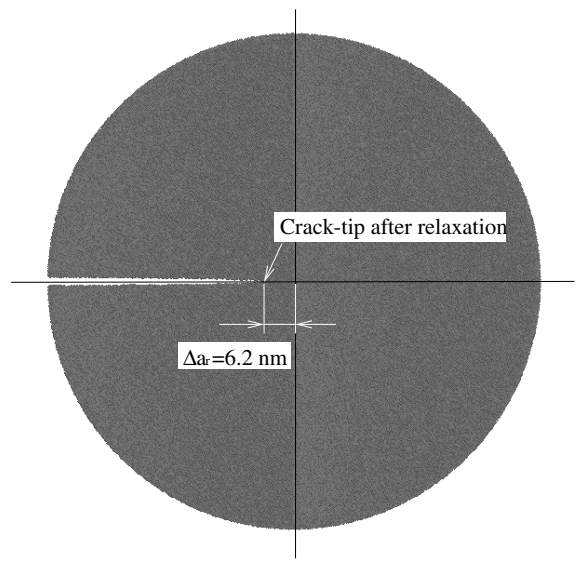


Figure 2 : Initial state

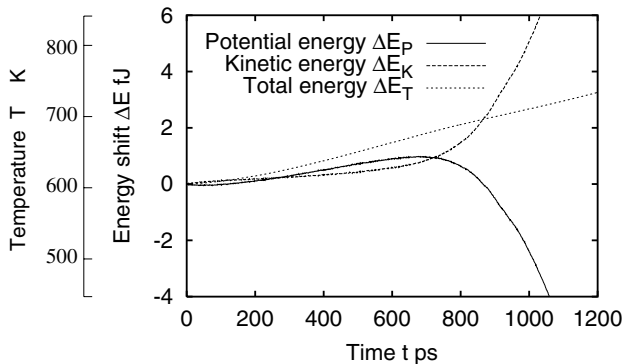


Figure 3 : Change of energy from the initial state

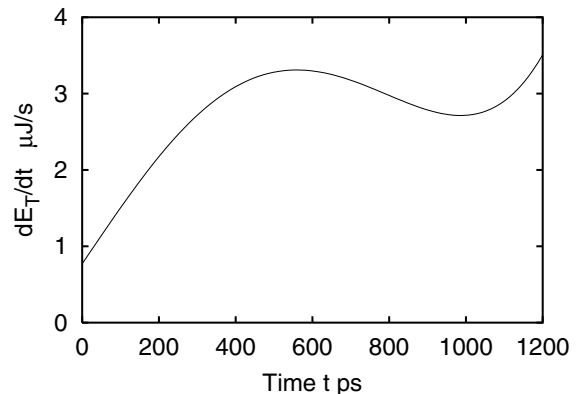


Figure 4 : Derivative of  $E_T$

goes up to  $T = 1000$  K or even higher. This is caused by the crystallization around the crack-tip.

The change of the total energy rate (*i.e.* the external power profile) is shown in Figure 4. Initially it monotonically increases, followed by the decrease and subsequently increases again at around  $t = 1000$  ps. As shown later, crystallization progresses during the external work rate is decreasing, and the most of it is completed before the external work rate recovers to rise again.

### 3.2 Change of deformation state

In order to show effectively the crystal formation around the crack-area and pertinent phenomena such as the grain

growth and possible dislocations in it, the changes of the strain over the time interval of 10 ps are demonstrated. Thus shapes of the crack and the distributions of the equivalent strain increment  $\Delta\bar{\epsilon}$  are shown for the crack-tip area of about 80 nm side in Figure 5. In order to observe microscopic deformation characteristics, the local values of strain are evaluated with the use of a weighted means scheme [Matsumoto, Kitagawa, Nakatani, and Nakatani (2001)]. The procedure is similar to the estimation method of strain used in Smoothed Particle Hydrodynamics (SPH) [Monaghan (1992)]. During the amorphous state, the process zone is deformed due to the generation and disappearance of the severely deformed local zones time by time. The crack opens in a similar fashion with smooth and round surfaces. Some circular spots with suppressed deformation appear in the vicinity

of the crack-tip at about 600 ps followed by rapid growth under the increasing severe stress situation. These regions are of crystalline phase (having different orientation of crystal lattice shown in Fig. 6 in different colors). During the stage, the distribution pattern of the deformation zones are significantly altered, as they grow. The particles stay elastic while they remain relatively small. This is because, perfect crystals have higher yield stress than that of the amorphous phase and the interaction between particles are small because of their sparse distribution. Most amorphous-crystal interfaces have large strain increment due to the phase transition.

After the crystal phase covers the crack-tip surfaces, the deformation mechanism changes into the mechanism associated with dislocation movement, grain sliding and grain-migration. Some dislocations are emanated from a triple point of grain boundary near the crack-tip(Fig.5(vi)).

### 3.3 Crystallization behavior

Figure 6 shows the distributions of bcc-structure at every 100 ps after 600 ps. Voronoi's polyhedra which are estimated at the instantaneous snapshots are used to pick up the bcc-structure. In order to distinguish each grain, all displayed atoms are colored by lattice orientation. The solid lines indicate the crack surface configuration. Some clusters nucleate, and most of all are opposite to each other across the crack line in the vicinity of the crack-tip. They have a rapid growth velocity. The grain size is small near the crack-tip, and it appears gradually large as it separates from the crack-tip. The smallest grain is smaller than 10 nm. The shape of region of the crystalline phase corresponds to the high stress region under this simulation condition(Fig.6(v)(vi)).

### 3.4 Distribution of temperature and equivalent strain

Figures 7 and 8 show the temperature distribution and equivalent strain distribution, respectively. At  $t \simeq 600$  ps, when the crystallization begin, although the temperature rise and deformation concentration at the crack tip region are observed, a remarkable change is not seen in the outer region (See Fig.7(i) and Fig.8(i)). As shown in Fig.6, the initial crystal nucleation position is not on the crack-tip surfaces but inside of the material. This result suggests that the crystal nucleation rate and crystal growth velocity are dependent not only on temperature but also on stress, strain-rate and other deformation state

intricately. Remarkable temperature rise accompanied by the crystallization was observed.

### 3.5 Change of crack tip opening displacement (CTOD) and crack extension

Figure 9 shows the change of the crack extension  $\Delta a$  and the crack-tip opening displacement (CTOD)  $b$ . The amount of crack extension was evaluated on the basis of the crack-tip position after the relaxation (Figure 2). The stress intensity factor  $K^I$  of each time is also shown in the horizontal axis. Roughly speaking amorphous metal behaves like a perfect plastic material, the figure also gives CTOD  $b_D$  obtained from Dugdale's model in plane strain. Here, we used  $\sigma_Y = 1.8$  GPa as a yield stress. It was evaluated from the equivalent stress at the crack-tip region averaged from  $t = 400$  ps to  $t = 600$  ps. In the amorphous state, it turns out that CTOD obtained from MD analysis  $b$  agrees with Dugdale's model  $b_D$  very well. Similar results have been obtained experimentally [Flores and Dauskardt (1999)]. The amount of the crack extension  $\Delta a$  increases monotonously. However, after  $t = 900$  ps, since the crack front region changes to polycrystalline structures, the amount of the crack extension  $\Delta a$  and CTOD increase become small.

### 3.6 Stress distribution in front of the crack tip

The distribution of the hoop stress in the crack plane ( $\sigma_\theta$ ) is shown in Fig. 10. Along the horizontal axis, the distance from the crack-tip at each time is taken, and the distance normalized by CTOD is also shown simultaneously. The dotted line in each figure shows the linear elastic solution obtained from the stress intensity factor  $K^I$  at each time. During the amorphous state, we can find that the linear elastic solution agrees with the result of the MD analysis very well in the region  $r/b > 2$ . The peak of the stress which exists around  $r/b \simeq 1$  until  $t = 600$  ps gradually vanishes as crystal phase grows, and the stress distribution becomes flat and the value becomes small rather than the linear elastic solution (see. Fig. 10(iv)). We suppose that it is caused mainly by the deformation accompanied by the crystallization. The stress increases again when crystallization around the crack-tip finishes mostly (see. Fig. 10(vi)). This is because, the nanocrystalline phase has higher yield stress than amorphous phase.

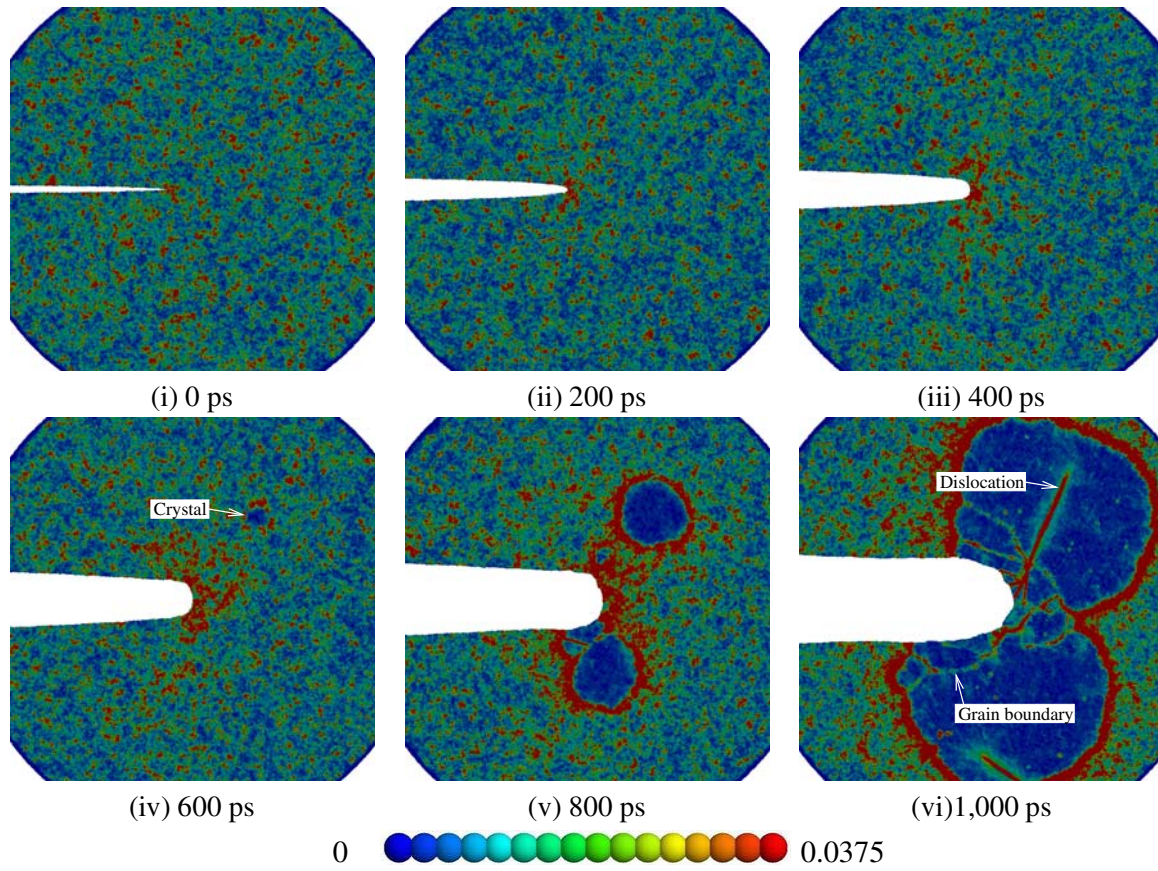


**Figure 5 :** Distribution of the equivalent strain increment  $\Delta\bar{\epsilon}$

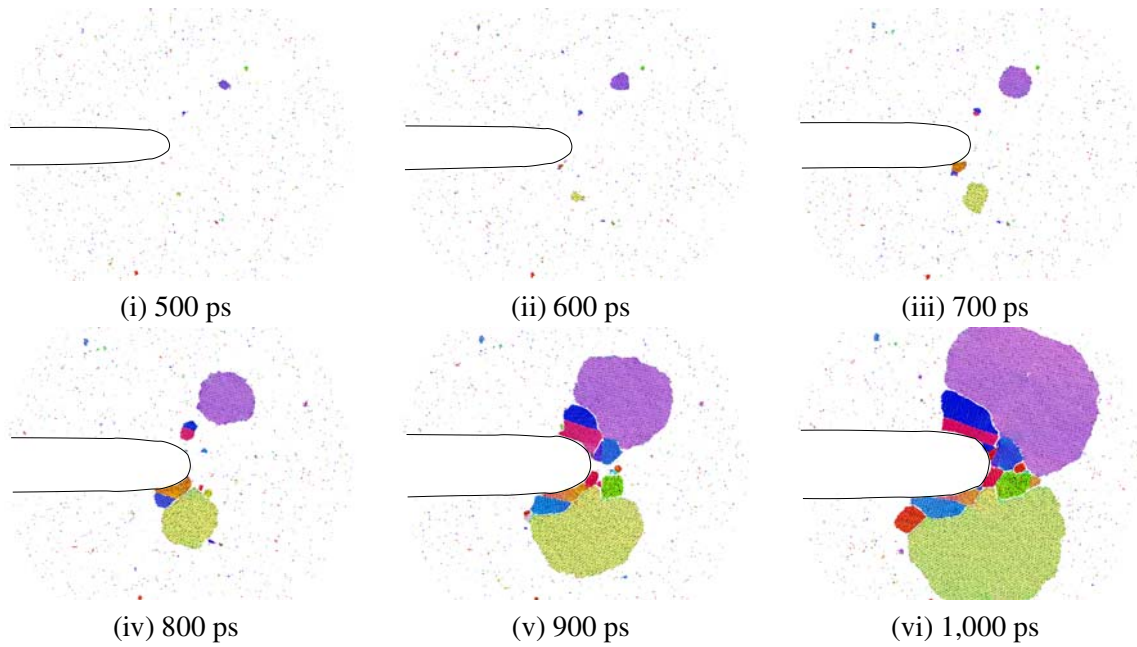


**Figure 6 :** Distribution of bcc structure

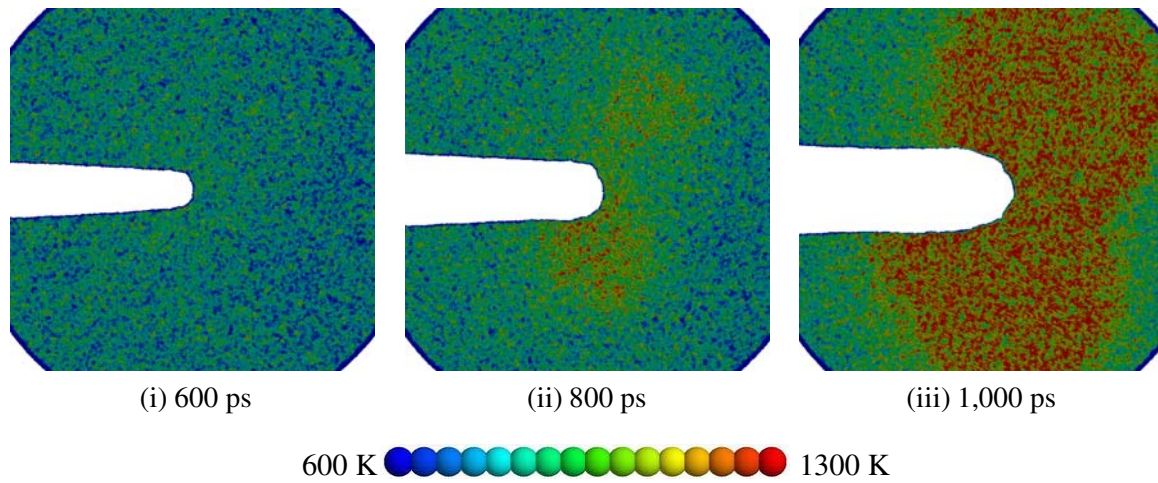


Figure 7 : Temperature distribution

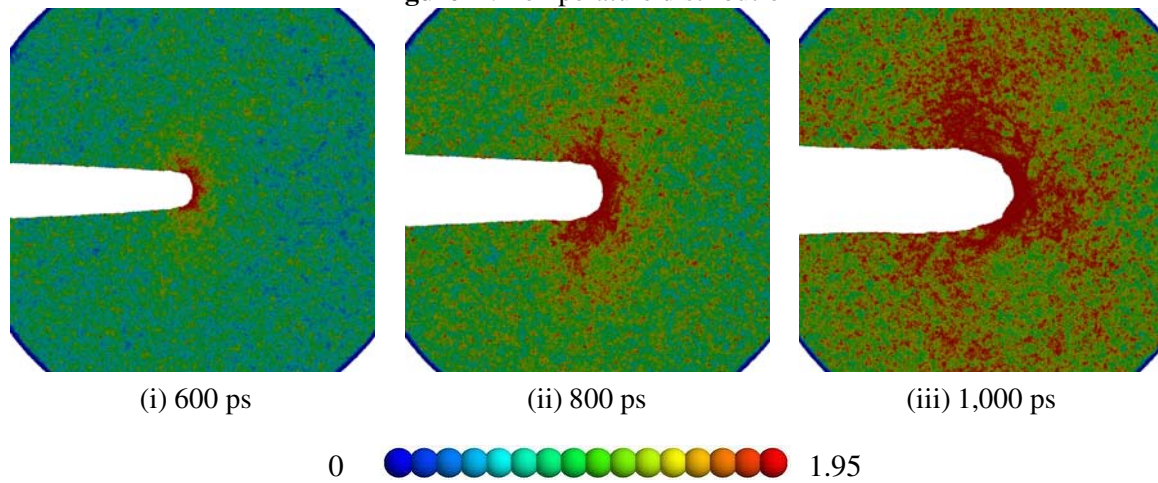


Figure 8 : Distribution of the equivalent strain  $\bar{\epsilon}$

#### 4 Conclusions

We performed a large scale MD simulation of crack growth in an amorphous metal in order to investigate the internal structure change around the crack-tip and its influence on the crack extension behavior and deformation state.

- Amorphous metal is crystallized by severe deformation around the crack tip. The distribution of deformation zones and the deformation mechanism are significantly altered, as crystalline phase grows.
- The stress in the crack front decreases temporarily by the deformation accompanied by the crystallization. The stress increases again when crystallization around the crack-tip finishes mostly.

- The grains are not deformed while they remain relatively small. After the crystal phase covers the crack-tip surfaces, it is deformed by dislocation and grain boundary based mechanism.
- As it is pointed out from before [Nakatani, Nakatani, Sugiyama, and Kitagawa (2000); Flores and Dauskardt (1999)], Dugdale's model can provide a good approximation during amorphous state. However it is risky to apply it to the problem which has the possibility of crystallization.

In this paper, the simulation was carried out by use of pure Fe amorphous. It is thought there are some common aspects on the effects of crystallization to crack growth behavior, stress distribution and deformation state around the crack-tip between the pure component amorphous and multi-component amorphous.

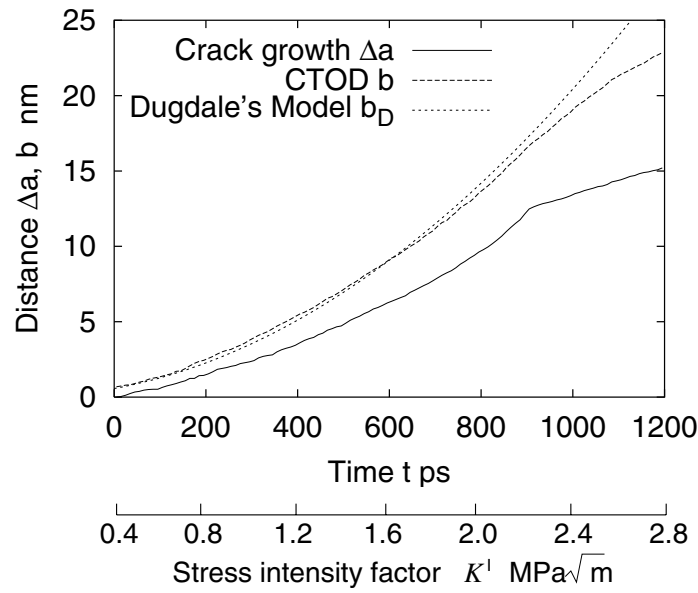


Figure 9 : Crack extension  $\Delta a$  and CTOD  $b$

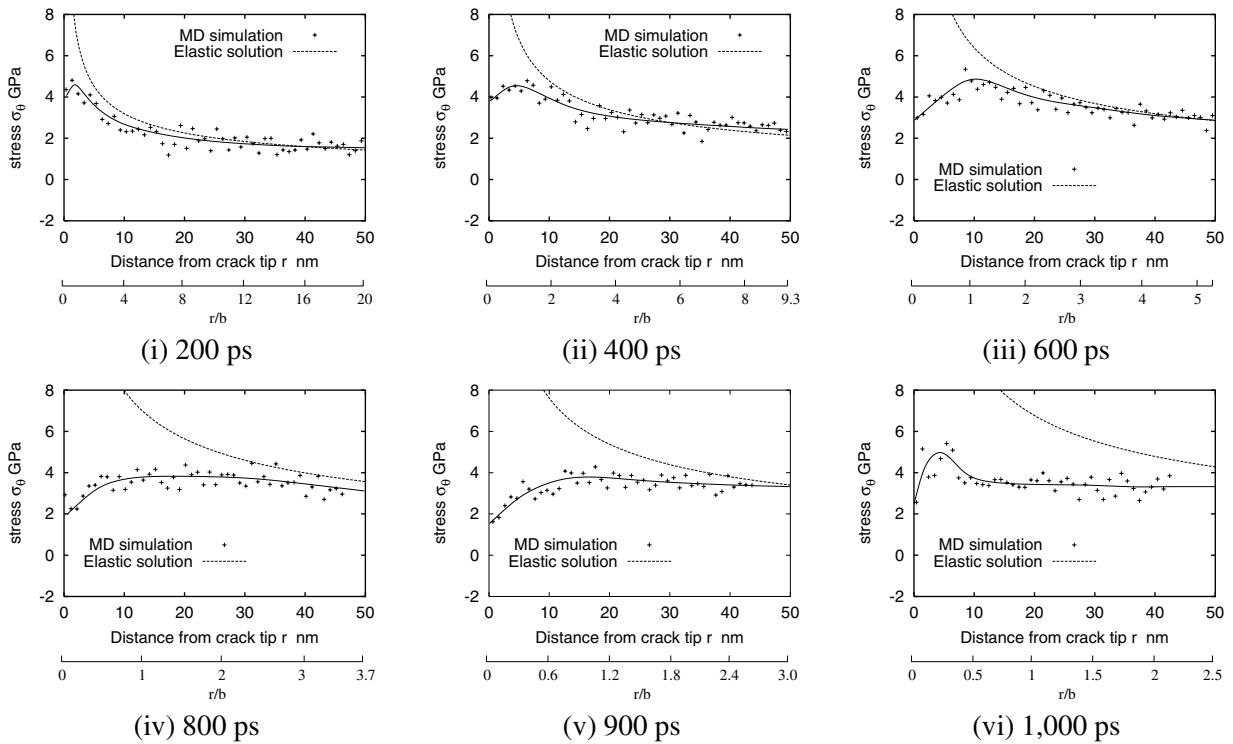


Figure 10 : Stress distribution in front of the crack-tip

**Acknowledgement:** This study was partly supported by Grant-in-Aid for Scientific Research from Ministry of Education, Culture, Sports, Science and Technology, Japan. Authors gratefully appreciate support from New Energy and Industrial Technology Development Organization (NEDO) of Japan and support from the Handai Frontier Research Center (FRC) supported by the Japanese Government's Special Coordination Fund for Promoting Science and Technology.

## References

- Abraham, F. F.** (2000): Maadly spanning the length scales in dynamic fracture. *CMES: Computer Modeling in Engineering & Sciences*, vol. 1, no. 4, pp. 63–70.
- Buehler, M. J.; Abraham, F. F.; Gao, H.** (2003): Hyperelasticity governs dynamic fracture at a critical length scale. *Nature*, vol. 426, no. 13, pp. 141–146.
- Conner, R. D.; Dandliker, R. B.; Johnson, W. L.** (1998): Mechanical properties of tungsten and steel fiber reinforced  $Zr_{41.25} Ti_{13.75} Cu_{12.5} Ni_{10} Be_{22.5}$  metallic glass matrix composites. *Acta Mater.*, vol. 46, pp. 6089–6102.
- Finnis, M. W.; Sinclair, J. E.** (1984): A simple empirical  $n$ -body potential for transition metals. *Philos. Mag., A*, vol. 50, no. 653, pp. 45–55.
- Finnis, M. W.; Sinclair, J. E.** (1986): Erratum. *Philos. Mag., A*, vol. 53, no. 1, pp. 161.
- Flores, K. M.; Dauskardt, R. H.** (1999): Local heating associated with crack tip plasticity in  $Zr-Ti-Ni-Cu-Be$  bulk amorphous metals. *J. Mater. Res.*, vol. 14, no. 3, pp. 638–643.
- Gao, M. C.; Hackenberg, R. E.; Shiflet, G. J.** (2001): Deformation-induced nanocrystal precipitation in  $Al$ -base metallic glasses. *Mater. Trans.*, vol. 42, pp. 1741.
- Honeycutt, J. D.; Andersen, H. C.** (1988): Molecular dynamics study of melting and freezing of small Lennard-Jones clusters. *J. Phys. Chem.*, vol. 91, pp. 4950–4963.
- Inoue, A.** (2000): Stabilization of metallic supercooled liquid and bulk amorphous alloys. *Acta Mater.*, vol. 48, pp. 279–306.
- Inoue, A.; Nakazato, K.; Kawamura, Y.; Masumoto, T.** (1994): The effect of additional  $Cu$  element on the structure and mechanical properties of  $Al-Ni-M$  ( $M=Co$  and  $Ni$ ) amorphous alloys containing nanoscale  $fcc-Al$  particles. *Mater. Sci. Eng.*, pp. 654–658.
- Kalia, R. K.; Nakano, A.; Vashishta, P.; Rountree, C. L.; Van Brutzel, L.; Ogata, S.** (2003): Multiresolution atomistic simulations of dynamic fracture in nanostructured ceramics and glasses. *Int. J. Fracture*, vol. 121, pp. 71–79.
- Lee, B. J.; Baskes, M. I.; Kim, H.; Cho, Y. K.** (2001): Second nearest-neighbor modified embedded atom method potential for  $bcc$  transition metals. *Phys. Rev. B*, vol. 64, no. 18, pp. 184102.
- Lee, B. J.; Lee, C. S.; Lee, J. C.** (2003): Stress induced crystallization of amorphous materials and mechanical properties of nanocrystalline materials: a molecular dynamics simulation study. *Acta Mater.*, vol. 51, pp. 6233–6240.
- Lee, J. C.; Kim, Y. C.; Ahn, J. P.; Kim, J. P.; Lee, S. H.; Lee, B. J.** (2004): Deformation-induced nanocrystallization and its influence on work hardening in a bulk matrix composite. *Acta Mater.*, vol. 52, pp. 1525–1533.
- Li, J.; Yip, S.** (2002): Atomistic measures of materials strength. *CMES: Computer Modeling in Engineering & Sciences*, vol. 3, no. 2, pp. 219–227.
- Matsumoto, R.; Kitagawa, H.; Nakatani, A.** (2002): Molecular dynamics simulation of deformation-induced nanocrystallization process in amorphous metal. *Proceeding of International Conference on Computational Engineering & Science 2002(ICES'02), USA, Reno, 31st Jul-2nd Aug. (CD-ROM)*.
- Matsumoto, R.; Kitagawa, H.; Nakatani, A.** (2003): Molecular dynamics simulation of deformation-induced nanocrystallization in an amorphous metal. *J. Soc. of Mat. Sci. Japan*, vol. 52, no. 3, pp. 235–240 (in Japanese).
- Matsumoto, R.; Kitagawa, H.; Nakatani, A.** (2003): Molecular dynamics study on hydrostatic effect on crystal nucleation rate and growth velocity in amorphous metal. *Proceeding of International Conference on Computational & Experimental Engineering and Science*

2003(ICCES'03), Greece, Corfu, 25th-29th Jul. (CD-ROM).

**Matsumoto, R.; Kitagawa, H.; Nakatani, K.; Nakatani, A.** (2001): Atomistic analysis of crack propagation in amorphous metal. *Trans. JSME, A*, vol. 67, no. 1, pp. 23–29(in japanese).

**Matsumoto, R.; Nakatani, A.; Kitagawa, H.** (2003): Analysis of crack opening behavior in amorphous metal(comparative study of atomistic and elastoviscoplastic continuum model). *Trans. JSME, A*, vol. 69, no. 7, pp. 1074–1081(in japanese).

**Monaghan, J. J.** (1992): Smoothed particle hydrodynamics. *Annu. Rev. Astron. Astrophys.*, vol. 30, pp. 543–574.

**Nakatani, A.; Shimokawa, T.; Matsumoto, R.; Kitagawa, H.** (2004): Atomistic study on ideal strength of nanocrystal and deformation induced nanostructures. *IUTAM Symposium on Mesoscopic Dynamics of Fracture Process and Materials Strength (eds. H. Kitagawa and Y. Shibutani, published from KLUWER ACADEMIC PUBLISHERS)*, pp. 365–380.

**Nakatani, K.; Kitagawa, H.; Nakatani, A.** (1997): Molecular dynamics simulation on the mechanical strength of one-component amorphous metal — decreasing of elastic moduli and strength induced by change of internal structure. *J. Soc. of Mat. Sci. Japan*, vol. 46, no. 3, pp. 244–249(in japanese).

**Nakatani, K.; Nakatani, A.; Sugiyama, Y.; Kitagawa, H.** (2000): Molecular dynamics study on mechanical properties and fracture in amorphous metal. *AIAA Journal*, vol. 38, no. 4, pp. 695–701.

**Nieh, T. G.; Wadsworth, J.; Liu, C. T.; Ohkubo, T.; Hirotsu, Y.** (2001): Plasticity and structural instability in a bulk metallic glass deformed in the supercooled liquid region. *Acta Mater.*, vol. 49, no. 15, pp. 2887–2896.

**Nishimura, K.; Miyazaki, N.** (2001): Molecular dynamics simulation of crack propagation in polycrystalline material. *CMES: Computer Modeling in Engineering & Sciences*, vol. 2, no. 2, pp. 143–154.

**Ogura, A.; Sato, M.; Tarumi, R.; Shimojo, M.; Takashima, K.; Higo, Y.** (2001): Formation of nano-sized crystals during plastic deformation in amorphous alloys. *Mat. Res. Soc. Symp. Proc.*, vol. 634, pp. B1.10.1.

**Parrinello, M.; Rahman, A.** (1981): Polymorphic transitions in single crystals: a new molecular dynamics method. *J. Appl. Phys.*, vol. 52, no. 12, pp. 7812–7190.

**Schiøtz, J.; Jacobsen, K. W.** (2003): A maximum in the strength of nanocrystalline copper. *Science*, vol. 301, pp. 1357–1359.

**Schiøtz, J.; Tolla, F. D. D.; Jacobsen, K. W.** (1998): Softening of nanocrystalline metals at very small grain sizes. *Nature*, vol. 391, no. 5, pp. 561–563.

**Shastry, V.; Farkas, D.** (1996): Molecular statics simulation of fracture in  $\alpha$ -iron. *Modelling Simul. Mater. Sci. Eng.*, vol. 4, pp. 473–492.

**Shen, S.; Atluri, S. N.** (2004): Atomic-level stress calculation. *Proceeding of the 2004 International Conference on Computational & Experimental Engineering & Science*, pp. 1541–1547.

**Shen, S.; Atluri, S. N.** (2004): Atomic-level stress calculation and continuum-molecular system equivalence. *CMES: Computer Modeling in Engineering & Sciences*, vol. 6, no. 1, pp. 91–104.

**Shen, S.; Atluri, S. N.** (2004): Multiscale simulation based on the meshless local petrov-galerkin(mlpg) method. *CMES: Computer Modeling in Engineering & Sciences*, vol. 5, no. 3, pp. 235–256.

**Verlet, L.** (1967): Computer "experiments" on classical fluids. i. thermodynamical properties of lennard-jones molecules. *Phys. Rev. B*, vol. 151, no. 1, pp. 98–103.

**Yoshizawa, Y.; Oguma, S.; Yamauchi, K.** (1988): New fe-based soft magnetic alloys composed of ultrafine grain structure. *J. Appl. Phys.*, vol. 64, pp. 6044–6046.